A MATHEMATICAL MODEL OF A GAUZE REACTOR FOR THE AMMONIA OXIDATION

Vlastimil FILA and Bohumil BERNAUER

Department of Inorganic Technology,
Prague Institute of Chemical Technology, 166 28 Prague 6, The Czech Republic

Received April 7, 1993
Accepted August 13, 1993

The behaviour of an industrial reactor for the oxidation of ammonia with Pt–Rh gauzes was simulated by means of a mathematical model accounting for the axial dispersion of the components, radiative heat transmission in the reactor, and the effect of temperature on the physico-chemical properties of the reacting mixture. The effect of the preheating temperature, the input mixture composition, pressure and reactor load on the temperature distribution in the catalyst bed and on the NO yield was examined. The calculated NO yields agree well with the values actually attained in industrial reactors. The effect of the reaction mixture composition and total pressure on the yield is also consistent with observed dependences.

Reactors containing a catalyst in the form of a gauze are applied to the production of HCN from CH_4, NH_3 and O_2 (the Andrussow process) as well as to the preparation of oxides of nitrogen during the production of nitric acid (the Ostwald process).

In dependence on the catalyst used and on the process conditions (temperature, pressure, gas phase composition), the catalytic oxidation of NH_3 can generally involve the following reactions.

$$4\ NH_3 + 5\ O_2 \longrightarrow 4\ NO + 6\ H_2O \qquad \Delta H^0_{298} = -907.28\ \text{kJ} \qquad (A)$$

$$4\ NH_3 + 4\ O_2 \longrightarrow 2\ N_2O + 6\ H_2O \qquad \Delta H^0_{298} = -1\ 104.9\ \text{kJ} \qquad (B)$$

$$4\ NH_3 + 3\ O_2 \longrightarrow 2\ N_2 + 6\ H_2O \qquad \Delta H^0_{298} = -1\ 269.02\ \text{kJ} \qquad (C)$$

In addition, the following processes also play a minor role.

$$2\ NH_3 \rightleftharpoons N_2 + 3\ H_2 \qquad \Delta H^0_{298} = 91.94\ \text{kJ} \qquad (D)$$

$$2\ NO \longrightarrow N_2 + O_2 \qquad \Delta H^0_{298} = -180.62\ kJ \qquad (E)$$

$$4\ NH_3 + 6\ NO \longrightarrow 5\ N_2 + 6\ H_2O \qquad \Delta H^0_{298} = -1\ 808.28\ kJ \qquad (F)$$

The total pressure during the combustion of NH_3 is the most important technological parameter of industrial oxidation of ammonia[1 – 4]. Oxidation of NH_3 occurs at normal (0.1 MPa) as well as elevated pressures. In the former case the working temperature in the catalyst bed is about 820 °C, and increases with increasing pressure[2,5] to reach approximately 940 °C at 0.8 MPa.

The concentration of NH_3 in the entering air–ammonia mixture is typically 9.5 – 11.5 vol.%, the time of contact with the catalyst is 10^{-3} – 10^{-4} s. The platinum catalyst, which is usually an alloy with rhodium (2 – 10%), has the form of gauzes made up of wires 0.04 – 0.09 mm in diameter, the gauze density is 1 024 – 3 600 mesh cm^{-2}. The surface density is typically[2,4,6] 0.5 – 0.9 kg m^{-2}.

The objective of the present work was to set up an appropriate mathematical model of a reactor for the oxidation of ammonia on Pt–Rh gauzes. The model should account for the following basic features of the process:

– increase in the NO yield if the specific surface area of the catalyst is increased;
– decrease in the reaction selectivity with respect to NO if the total pressure in the reactor is increased;
– decrease in the NO yield if the concentration of NH_3 in the feed is increased.

The model should also provide data of NO yields, total NH_3 conversion degrees and reaction mixture temperatures which should agree reasonably well with experimental data.

The reactor for the oxidation of ammonia considered is shown in Fig. 1. It can be separated into three segments. The first segment includes a conical adapter with inlet

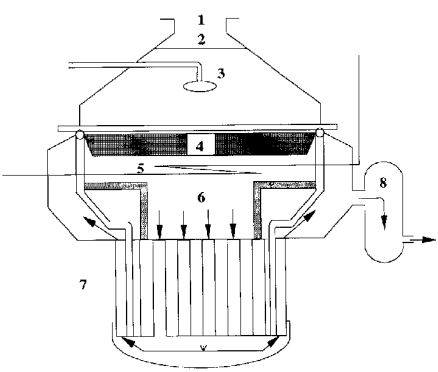

FIG. 1
Layout of the NH_3 oxidation reactor. 1 Opening for feeding in the ammonia-air mixture, 2 perforated plate, 3 device for starting catalyst heating, 4 basket carrying Pt–Rh gauzes, 5 steam overheater, 6 outlet into steam boiler, 7 steam boiler, 8 economizer

pipe, which serves the distribution and preheating of the input mixture. The second segment, having a cylindrical shape, accommodates the catalyst gauzes. The third segment has also a conical shape and ends in the compartment of the steam boiler tubes to recuperate the reaction heat.

Before entering the reactor, the air–ammonia mixture is preheated to 130 – 150 °C in a heat exchanger. The conical part of the reactor contains a perforated plate which facilitates a good distribution of the gas along the entire cross-section of the Pt–Rh gauzes. The mixture, heated by radiation from the first gauzes of the catalyst, is fed into the catalyst bed, where the reaction takes place. The nitrous gases at a high temperature (about 850 °C) pass through a layer of a filter mass which traps platinum, to reach the steam boiler compartment.

From the mathematical viewpoint, this reactor is a complex system involving several strongly exothermal reactions as well as transfer phenomena including heat transmission by radiation. When deriving equations of the mathematical model and solving them we proceeded from the requirement that the model be as simple as possible while meeting the above demands.

THEORETICAL

Kinetics of Ammonia Oxidation on Platinum

Older theories of oxidation of ammonia on platinum usually presumed that transient compounds are formed[7–9]. Such hypotheses, however, failed to prove true; experiments indicate that the reactions of components on the catalyst surface involve no transient compounds. The selectivity of the oxidation of NH_3 on Pt and the kinetics of oxidation on Pt, Rh, Pd have been studied by Pignet and Schmidt[10,11]. The authors performed experiments in a low-pressure reactor interfaced to a mass spectrometer and, based on the experimental data, suggested a simple series-parallel mechanism as follows, based on the concept by Fogel and coworkers[12].

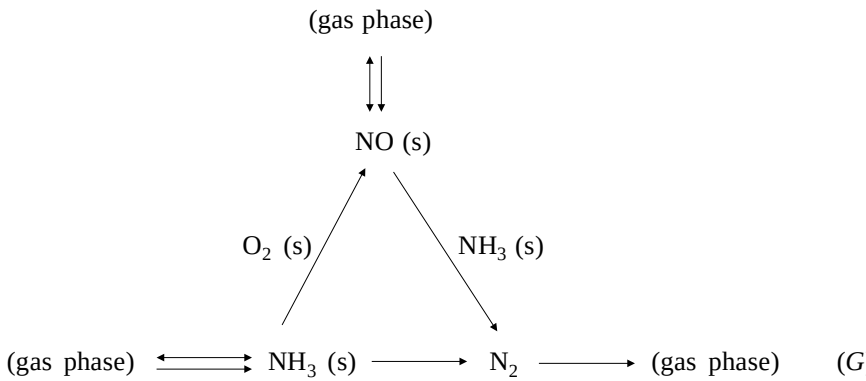

(*G*)

The following relations in ref.[11] give the rates of NO and N_2 formation.

$$r_{NO} = \frac{2.209 \,.\, 10^{-11} \exp\left(\frac{90\,791.6}{\boldsymbol{R}\, T_s}\right) p_{NH_3}\, p_{O_2}^{1/2}}{\left(1 + 6.928 \,.\, 10^{-3} \exp\left(\frac{1\,840.93}{\boldsymbol{R}\, T_s}\right) p_{O_2}^{1/2}\right)\left(1 + 1.2 \,.\, 10^{-5} \exp\left(\frac{106\,690.5}{\boldsymbol{R}\, T_s}\right) p_{NH_3}\right)} \qquad (1)$$

$$r_{N_2} = \frac{2.36 \,.\, 10^{-15} \exp\left(\frac{108\,782.5}{\boldsymbol{R}\, T_s}\right) p_{NH_3}\, p_{NO}}{\left(1 + 4.05 \,.\, 10^{-4} \exp\left(\frac{45\,605}{\boldsymbol{R}\, T_s}\right) p_{O_2} + 3.38 \,.\, 10^{-8} \exp\left(\frac{87\,444.4}{\boldsymbol{R}\, T_s}\right) p_{NH_3}\right)^2} +$$

$$+ \frac{1.65 \,.\, 10^{-8} \exp\left(\frac{-2\,385}{\boldsymbol{R}\, T_s}\right) p_{NH_3}}{1 + 4.05 \,.\, 10^{-4} \exp\left(\frac{45\,605}{\boldsymbol{R}\, T_s}\right) p_{O_2} + 3.38 \,.\, 10^{-8} \exp\left(\frac{87\,444.4}{\boldsymbol{R}\, T_s}\right) p_{NH_3}} \qquad (2)$$

(If the partial pressures are in Pa, the reaction rates are in mol s^{-1} per cm^2 of reacting surface.)

The kinetic parameters in equations (*1*), (*2*) were obtained[11] from the experimental data measured at low pressures (not exceeding 15 Pa). The application of the above kinetic equations to the calculation of reactors working at atmospheric or elevated pressures is warranted to some degree with regard to the existing strong effect of outer diffusion on the total reaction rates and the related substantial decrease in the concentrations of the reactants on the catalyst surface. In conventional conditions of industrial application of the Pt–Rh catalyst, the ratio of ammonia partial pressure in the gas phase and at the catalyst surface is on the order of 10^{-4}.

The explanation of the negative effect of total pressure on the NO yield in industrial converters lies in reaction (*F*) between NH_3 and NO in the gas phase, whose kinetics has been examined by Wise and Frech[13]. Based on their experiments in which they monitored the time behaviour of the total gas pressure in the apparatus due to reaction (*F*) the authors derived the equation

$$\frac{dP}{dt} = k\, p_{NH_3}\, p_{NO}^{-1/2}\,, \qquad (3)$$

where

$$k = 9.527 \cdot 10^9 \exp(-229\,018/\boldsymbol{R}T) \qquad (\mathrm{Pa}^{1/2}\,\mathrm{s}^{-1})\,. \qquad (4)$$

Equations (*1*) – (*3*) constitute the only known mathematical representation of kinetics of oxidation of NH_3 on Pt gauzes at 600 – 1 200 K, and therefore we employed them when modelling the industrial reactor for the oxidation of NH_3.

Model of the Reactor

The following assumptions were made when setting up equations of the mathematical model:

1. Temperatures and component concentrations are constant in the radial direction.
2. The gauzes follow each other closely and the total length of the catalytically active zone is $L = n_L(r_w + r_s)$.
3. The catalyst properties do not vary with time.
4. Preheating of the reaction mixture by partial absorption of thermal radiation from the catalyst bed front is allowed for in the first reactor segment.
5. The gas phase exhibits ideal behaviour of state.
6. Heat transfer by radiation takes place from the catalyst bed front and end into the space before and after the bed.

The balance of the *i*-th component in the gas phase (i = NH_3, O_2, NO) then can be represented as

$$\frac{\mathrm{d}(v\,c_i)}{\mathrm{d}z} - E_i\,\frac{\mathrm{d}^2 c_i}{\mathrm{d}z^2} = \frac{a_V\,\beta_i}{\gamma}\,(c_{s,i} - c_i) + \sum_{j=1}^{N} R_{g,j}\,\nu_{i,j} \qquad (5)$$

and the following relation applies to the gas–solid interface:

$$S_g\,\rho_c \sum_{j=1}^{N} R_{s,j}\,\nu_{i,j} + \beta_i\,\frac{a_V}{1-\gamma}\,(c_i - c_{s,i}) = 0\,. \qquad (6)$$

The enthalpy balance of the gas phase, including the heat transfer between the catalyst and the gas phase, heat dissipation in the environment, and heat generation by the gas phase reaction, can be written as

$$\frac{\mathrm{d}(v\,\rho c_{pf} T)}{\mathrm{d}z} = \frac{\alpha_{fc}\,a_V}{\gamma}\,(T_s - T) + \frac{2\,k_{fo}}{r_1}\,(T_o - T) + \sum_{j=1}^{N} R_{g,j}\,(-\Delta H r_j)\,, \qquad (7)$$

whereas the enthalpy balance of the catalyst, including the heat transfer in the catalyst bed, heat transfer between the catalyst and the gas phase, and heat generation by reaction on the catalyst surface, is

$$\lambda_{ef} \frac{d^2T_s}{dz^2} + \frac{a_V}{1-\gamma} \alpha_{fc} (T - T_s) + S_g \rho_c \sum_{j=1}^{N} R_{s,j} (-\Delta Hr_j) = 0 . \qquad (8)$$

The boundary conditions for the component concentrations are based on the equal component fluxes at the two ends of the catalyst layer, $z = 0$ and $z = L$ (Fig. 2), and can be written in the form

$$\left(\frac{dc_i}{dz}\right)_{z=0} = - \frac{A_1 v^0 c_i^0}{\Pi r_1^2 \gamma E_i} + \frac{v(0)\, c_i(0)}{E_i} \qquad (9)$$

$$\left(\frac{dc_i}{dz}\right)_{z=L} = 0 , \qquad (10)$$

where

$$v(0) = \frac{A_1 T(0)}{\Pi r_1^2 \gamma T^0} v^0 . \qquad (11)$$

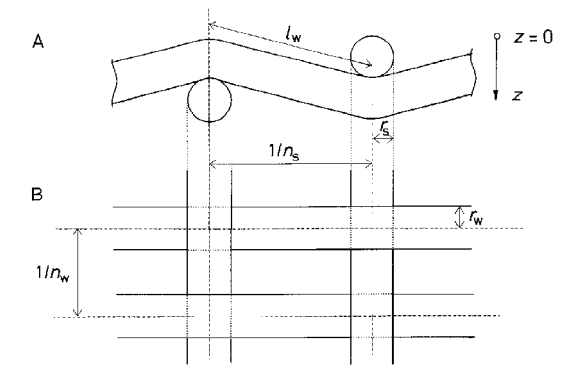

FIG. 2
Layout of the gauzes. A Section, B view in the gas flow direction

The reaction mixture entering into the conical part of the reactor is preheated by the radiant heat flux from the Pt–Rh gauzes. This fact is expressed through Eq. (*12*), which allows the starting gas phase temperature $T(0)$ at the catalyst layer front ($z = 0$) to be calculated:

$$T(0) = T^0 + \frac{\Pi r_1^2 (1 - \gamma) \sigma \varphi \varepsilon}{\dot{n}^0 c_p} \left[T_s(0)^4 - \left(\frac{T^0 + T_s(0)}{2} \right)^4 \right]. \qquad (12)$$

The boundary conditions for the catalyst temperature express the equal heat fluxes at $z = 0$ and $z = L$.

$$\left(\frac{dT_s}{dz} \right)_{z=0} = \frac{\sigma \varphi}{\lambda_{ef}} \left[T_s(0)^4 - \left(\frac{T^0 + T_s(0)}{2} \right)^4 \right] \qquad (13)$$

$$\left(\frac{dT_s}{dz} \right)_{z=L} = \frac{\sigma \varphi}{\lambda_{ef}} \left[\left(\frac{T_v^0 + T_s(L)}{2} \right)^4 - T_s(L)^4 \right] \qquad (14)$$

The concentration of component i in the gas phase was expressed via the mass fraction w_i, and the system of equations (*5*) – (*8*) was converted to a dimensionless form:

$$B_1 \frac{d^2 w_i}{dZ^2} + \frac{dw_i}{dZ} = B_2 C_{s,i} - B_3 w_i + B_4 \qquad (15)$$

$$B_5 C_{s,i} - B_6 w_i - B_7 = 0 \qquad (16)$$

$$\frac{dT}{dZ} = B_8 (T_s - T) + B_9 + B_{10} (T_0 - T) \qquad (17)$$

$$\frac{d^2 T_s}{dZ^2} + B_{11} (T - T_s) + B_{12} = 0, \qquad (18)$$

where the B_i's are as follows:

$$B_1 = -\frac{d_P}{Pe_a L} \qquad B_2 = \frac{a_V}{\gamma G}\ \beta_i\ M_i\ A\ c_i^0\ L \tag{19}$$

$$B_4 = \frac{1}{G}\ M_i\ A\ L \sum_{j=1}^{N} R_{g,j}\ \nu_{i,j} \tag{20}$$

$$B_3 = \frac{a_V}{\gamma \nu}\ \beta_i\ L \qquad B_5 = M_i\ A\ \beta_i\ \frac{a_V}{1-\gamma} \tag{21}$$

$$B_6 = \beta_i\ \frac{a_V}{1-\gamma}\ G\ \frac{1}{\nu\ c_i^0} \tag{22}$$

$$B_7 = \frac{M_i\ A\ S_g\ \rho_c\ (\nu_{i,1}\ R_{s,1} + \nu_{i,2}\ R_{s,2})}{c_i^0} \tag{23}$$

$$B_8 = \frac{\alpha_{fc}\, a_V\, L\, A}{\gamma\, c_{pf}\, G} \qquad B_9 = \frac{L\, A}{c_{pf}\, G} \sum_{j=1}^{N} R_{g,j}\ (-\Delta H r_j) \tag{24}$$

$$B_{10} = \frac{2\, k_{fo}\, L\ A}{c_{pf}\, G\ r_1} \qquad B_{11} = \frac{L^2\, a_V}{(1-\gamma)\, \lambda_{ef}}\ \alpha_{fc} \tag{25}$$

$$B_{12} = \frac{S_g\ \rho_c\ L^2}{\lambda_{ef}\ T_{ref}} \sum_{j=1}^{N} R_{s,j}\ (-\Delta\, H r_j)\,. \tag{26}$$

The boundary conditions (*9*), (*10*) take the form

$$\left(\frac{\mathrm{d}w_i}{\mathrm{d}Z}\right)_{Z=0} = \frac{L\ Pe_a}{d_P}\ (w_i(0) - w_i^0) \tag{27}$$

$$\left(\frac{\mathrm{d}w_i}{\mathrm{d}Z}\right)_{Z=1} = 0 \tag{28}$$

and Eq. (*12*) becomes

$$T(0) = T^0 + B_{13}\left[T_s(0)^4 - \left(\frac{T^0 + T_s(0)}{2}\right)^4\right] \tag{29}$$

with

$$B_{13} = \frac{\Pi\, r_1^2\,(1-\gamma)\,\sigma\,\varphi\,\varepsilon\,T_{ref}^3}{G\; c_{pf}}\,. \tag{30}$$

The following holds true for Eqs (*13*), (*14*)

$$\left(\frac{\mathrm{d}T_s}{\mathrm{d}Z}\right)_{Z=0} = \frac{\sigma\,\varphi\,L\,T_{ref}^3}{\lambda_{ef}}\left[T_s(0)^4 - \left(\frac{T^0 + T_s(0)}{2}\right)^4\right] \tag{31}$$

$$\left(\frac{\mathrm{d}T_s}{\mathrm{d}Z}\right)_{Z=1} = -\frac{\sigma\,\varphi\,L\,T_{ref}^3}{\lambda_{ef}}\left[T_s(1)^4 - \left(\frac{T_v^0 + T_s(1)}{2}\right)^4\right]\,. \tag{32}$$

Reactions (*A*) and (*C*), occurring on the catalyst surface, and the homogeneous reaction (*F*) are involved in the model with the bulk reaction, whereas reactions (*A*) and (*C*) solely are involved in the model without bulk reaction.

The following relations for the rates of the chemical reactions (*A*) and (*C*) ($R_{s,1}$, $R_{s,2}$) follow from their stoichiometries.

$$R_{s,1} = r_{NO} \tag{33}$$

$$R_{s,2} = 2\,r_{N_2} \tag{34}$$

Relations (*1*) and (*2*) were employed to calculate the *r* values.

Equation (*3*) was applied when calculating the rate of the homogeneous reaction (*F*), $R_{g,1}$.

The effective conductivity λ_{ef}, involving the effect of radiation in the catalyst bed, was calculated by using the relations recommended by the authors[14,15], viz.

$$\frac{\lambda_{ef}}{\lambda_f} = \left(\frac{\lambda_{ef}}{\lambda_f}\right)_{N_{Nu}} + 0.707\, N_{Nu}^{0.96} \left(\frac{\lambda_s}{\lambda_f}\right)^{1.11}, \qquad (35)$$

whereas the effective axial thermal conductivity without allowing for radiation, $(\lambda_{ef}/\lambda_f)_{N_{Nu}=0}$, was calculated by employing the recommended correlations[16].

In view of the high axial concentration gradients we can assume that axial dispersions of the reaction components play an important part in this system, and therefore this effect was taken into account in the model used (Eqs (*15*) – (*18*), (*27*) – (*32*)). According to Carberry[17], the dispersion coefficient obeys the relation

$$E_i = \frac{v\, d_P}{Pe_a}, \qquad Pe_a = \frac{2}{\gamma}. \qquad (36)$$

The mass transfer coefficients β_i and heat transfer coefficients α_{fc} for the gas phase and Pt–Rh gauze system in Eqs (*15*) – (*18*) were calculated from the *j*-factor following Sattefield and Cortez[18].

The heat transfer between the outer reactor jacket and the environment was assumed to proceed through free convection, and the empirical correlations[19] were used to calculate the heat transfer coefficient k_{fo} in Eq. (*9*).

Equations (*37*) and (*38*) have been derived[20] for the calculation of the outer geometrical surface area and volume of a gauze with a simple rectangular net with a surface area of 1 m^2 and height of 2 $(r_w + r_s)$.

$$l_s = \sqrt{(r_s + r_w)^2 + \left(\frac{1}{n_s}\right)^2} \qquad (37)$$

$$l_w = \sqrt{(r_s + r_w)^2 + \left(\frac{1}{n_w}\right)^2} \qquad (38)$$

The geometrical surface area and volume of the catalyst (per m^2 of the gauze) then are

$$S_K = 2\,\Pi\, n_s\, n_w\, (r_w\, l_w + r_s\, l_s) \qquad (39)$$

$$V_K = 2 \Pi n_s n_w (r_w^2 l_w + r_s^2 l_s) . \quad (40)$$

Solution of the Model Equations

The system of Eqs (*15*) – (*18*) along with the conditions (*27*) – (*32*) is a system of strongly nonlinear algebraic-differential equations with boundary conditions.
The system was solved by the method of global orthogonal collocation[21].

An approximate solution is assumed in the form

$$y(x) = \sum_{j=1}^{N} l_j(x) \; y(x_j) , \quad (41)$$

where $l_j(x)$ is the Lagrangian interpolation polynomial and $y(x_j)$ is the value of the dependent variable (composition, temperature) in collocation point x_j.

$$l_j(x) = \frac{P_N(x)}{(x - x_j) \, P_N(x_j)} \qquad P_N(x) = \prod_{k=1}^{N} (x - x_k) \quad (42)$$

The first and second derivatives of $y(x)$ in the collocation points $\{x_k\}_{k = 1,N}$ can be expressed as linear combinations of $y(x_j) = y_j$.

$$\left(\frac{dy}{dx}\right)_{x = x_k} = \sum_{j=1}^{N} A_{k,j} \; y_j \quad (43)$$

$$\left(\frac{d^2y}{dx^2}\right)_{x = x_k} = \sum_{j=1}^{N} B_{k,j} \; y_j \quad (44)$$

The coefficients $A_{k,j}$ and $B_{k,j}$, along with the collocation points $\{x_k\}_{k = 1,N}$, were generated by means of the published programs JCOBI and DFOPR (ref.[21]). Nine internal collocation points ($N = 11$) within the interval of $x \in (0,1)$ corresponding to the roots of the Legendre polynomial of the 9-th degree, were used in all calculations.

The physical properties of the gas mixture were calculated in each collocation point in dependence on composition and temperature using available correlations[22].

By inserting the relations (*43*), (*44*) in the initial algebraic-differential equations (*15*) – (*18*), (*27*) – (*32*) we obtain a system of strongly nonlinear algebraic equations, which is solved by the modified Gauss–Newton method.

RESULTS AND DISCUSSION

The results given in this section were calculated, unless stated otherwise, for the following input parameters corresponding to a medium-pressure nitric acid production unit:

Input mixture temperature 150 °C, pressure in reactor 0.4 MPa, reactor diameter 3.2 m, NH_3 content in the entering air–ammonia mixture 10.5 mole %, reactor load 0.095 kg NH_3 per second and m^2 of sieve (which corresponds to a daily output of 200 t of HNO_3), catalyst layer: 5 Pt–Rh gauzes (L = 0.6 mm; gauzes 1 024 mesh cm^{-2}, wire diameter 0.06 mm, specific surface area 0.105 $m^2\ g^{-1}$).

Simulation of the behaviour of the reactor provided information concerning the effect of operating parameters (starting feed temperature and composition, total pressure) on the nitric oxide yield X_{NO}.

Effect of Specific Surface Area

Typical morphological changes in the surface of the platinum catalyst are known to take place during the technological process of oxidation of NH_3 (ref.[23]), leading to increase in the catalyst surface area and in the NO yield. This phenomenon is taken into account in practice so that new, unused gauzes are inserted at the end of the reactor and in some time are moved towards the reactor head. In the model this fact was simulated by increasing the specific surface area of the catalyst (parameter S_g). The results obtained are consistent with data from practice, the NO yield increasing with increasing specific surface area of the catalyst (Figs 3 and 4). This increase in the NO yield can be explained in terms of reduction of the partial pressure of NH_3 at the catalyst surface due to a higher reaction rate and thereby a reduction in the rate of the catalytic reaction between NH_3 and NO giving rise to nitrogen.

Anderson[23] observed specific surface areas of old Pt–Rh gauzes which were about 20 to 30-fold higher than the geometrical surface area of new gauzes. Our model calculations were performed for specific surface areas approximately 50-fold larger than the geometrical surface area. In this case the simulation program provided NO yields and temperatures which approached reasonably well those obtained in industrial practice.

The temperature profiles of the gas phase change with increasing specific surface area of the catalyst (Fig. 5), which is due to the fact that if the specific surface area is low, the reaction of NH_3 with O_2 giving mainly N_2, which has a considerably higher

$-\Delta Hr$ value, occurs preferentially. The gas temperature increases monotonically in dependence on Z over the region examined.

The temperature profiles of the catalyst change appreciably with increasing specific surface area (Fig. 6). At low S_g values the catalyst temperature increases in the direction of the axial coordinates to attain its maximum on the last Pt–Rh gauzes. By increasing S_g the temperature peak shifts towards the beginning: the first Pt–Rh gauzes are hottest and the predominating fraction of NH_3 reacts on them (Fig. 3).

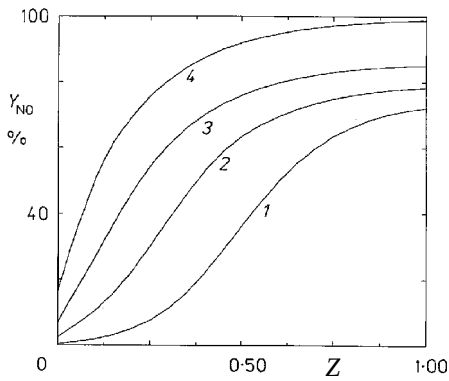

FIG. 3
Dependence of NO yield on the dimensionless axial coordinate (Z). Catalyst specific surface area S_g ($m^2\ g^{-1}$): *1* 0.055, *2* 0.060, *3* 0.065, *4* 0.155

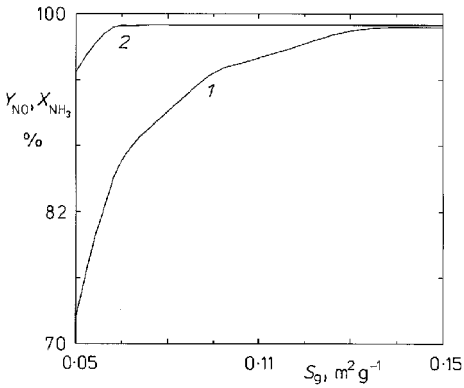

FIG. 4
Dependence of NO yield (*1*) ($z = L$) and conversion (*2*) on catalyst specific surface area

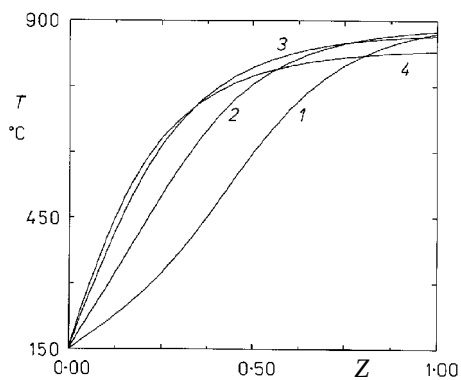

FIG. 5
Gas temperature profiles for various catalyst surface areas. Curve numbering as in Fig. 3

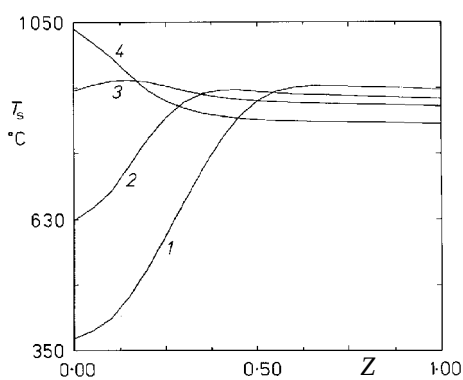

FIG. 6
Catalyst temperature profiles for various catalyst surface areas. Curve numbering as in Fig. 3

Effect of Input Mixture Composition

The effect of the concentration of NH_3 in the entering mixture on the NO yield has been determined experimentally by Atroshchenko and Kargin[1] for the ammonia–air mixture; the values are shown as squares in Fig. 7. The shape of this dependence was simulated both taking into account the NH_3 + NO bulk reaction and ignoring it (Fig. 7, curves *1* and *2*, respectively). The plot demonstrates that the calculated dependences agree well with the experiment, exhibiting a rapid drop near the air-to-ammonia stoichiometric point in reaction (*A*) (X^0 = 14.4 mole % NH_3).

The temperature profiles change as the entering mixture composition is varied. The development of temperature profiles in the catalyst bed is shown in Figs 8 and 9. The gas temperature increases monotonically in dependence on the relative coordinate in the catalyst bed. An inexpressive maximum in the gas temperature curve develops starting from concentrations in excess of 14 vol.% NH_3 (Fig. 8, curve *3*).

Figure 9 demonstrates that the catalyst temperature is significantly dependent on the axial coordinate in the reactor; the assumption of an isothermal course of the reaction, which is frequently applied, is apparently incorrect. Investigating losses of platinum on the gauzes, Zabryeski and Zmyslony[24] found the losses highest on the first gauzes, which is probably due to a higher temperature established in that part of the reactor.

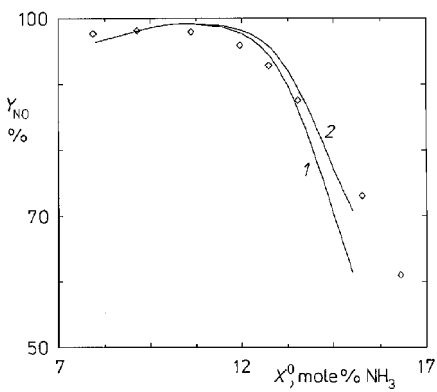

FIG. 7
Dependence of NO yield ($z = L$) on entering mixture composition for a daily output of 100 t HNO_3, p = 0.1 MPa, 3 Pt–Rh gauzes. Rectangles: empirical data[1], curves: *1* model taking account the bulk reaction, *2* model ignoring the bulk reaction

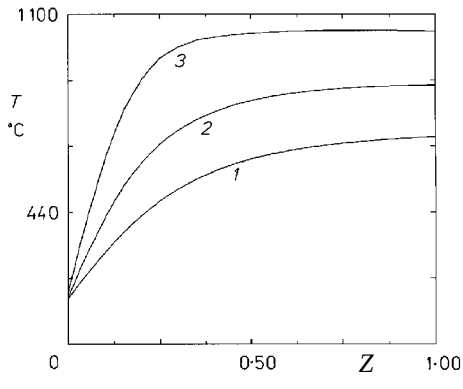

FIG. 8
Gas temperature profiles for various entering mixture composition values X^0 (mole % NH_3): *1* 8, *2* 11, *3* 14

Effect of Preheating Temperature on Yield

As the preheating temperature is increased, the NO yield as well as the total NH_3 conversion grows (Fig. 10), which is consistent with experimental observations (ref.[26], p. 53). If the preheating temperature is additionally increased to above 250 °C, the Y_{NO} value in industrial reactors decreases (ref.[26], p. 51). This may be due to a subsequent catalytic decomposition of NO at the gauzes as well as to a reaction of NH_3 at the metallic parts of the reactor body before coming in contact with the Pt–Rh gauzes. The calculated dependences of Y_{NO} on the preheating temperature are shown in Fig. 10 both taking into account and ignoring the NH_3 + NO reaction in the bulk (curves *1* and *2*, respectively). The shape of curve *1* approaches the experimental shape[26] and approximates well the preheating temperature optimum (about 250 °C). It can be thus concluded that the model involving the bulk reaction of NH_3 with NO fits the $Y_{NO}(T^0)$ well, although the reasons for the possible decrease in Y_{NO} may be more complex.

In industrial practice the feed temperature is a compromise having regard to the platinum loss increasing with temperature[24,25]; preheating temperatures of 150 – 200 °C are typically chosen.

Figure 11 shows that the gas phase temperature profiles are similar in all cases examined, whereas the solid phase temperature profiles exhibit a pronounced dependence on the axial coordinate (Fig. 12). According to ref.[1], the adiabatic temperature increase per mole % NH_3 in the entering mixture is about 70 °C. In all cases simulated, the gas

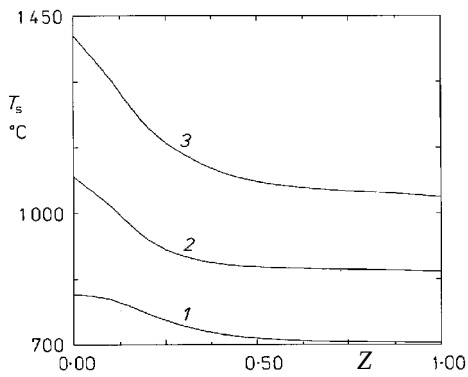

FIG. 9
Catalyst temperature profiles for various entering gas mixture compositions. Curves as in Fig. 8

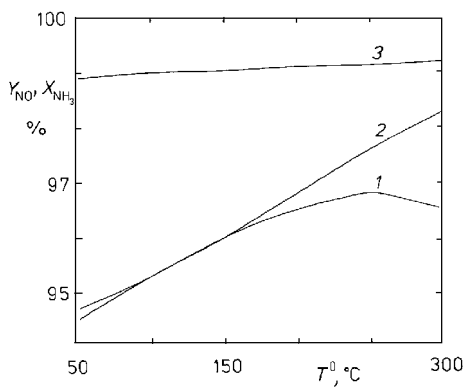

FIG. 10
Dependence of NO yield ($z = L$) (*1*, *2*) and total conversion (*3*) on entering mixture temperature using models involving (*1*) and ignoring (*2*) the bulk reaction (total conversion is identical for the two models)

temperature was 30 – 80 °C lower than the adiabatic reaction temperature due to heat dissipation into the environment. This is consistent with the values measured in industrial reactors[26].

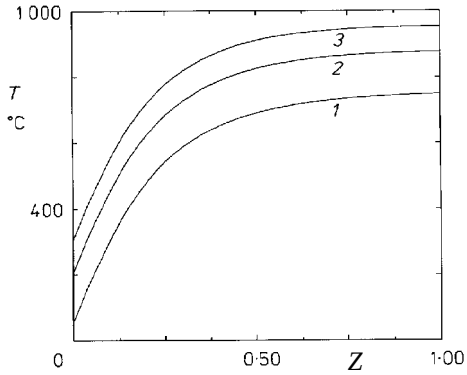

FIG. 11
Gas temperature profiles for various entering mixture temperatures T^0 (°C): *1* 50, *2* 200, *3* 300

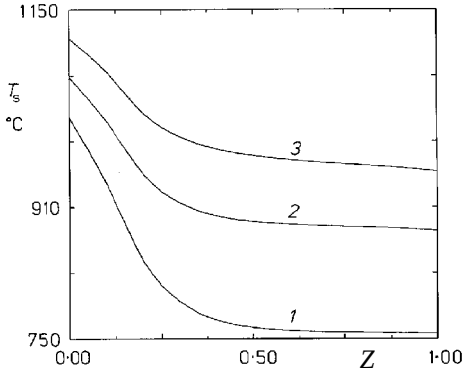

FIG. 12
Catalyst temperature profiles for various entering mixture temperatures. Curves as in Fig. 11

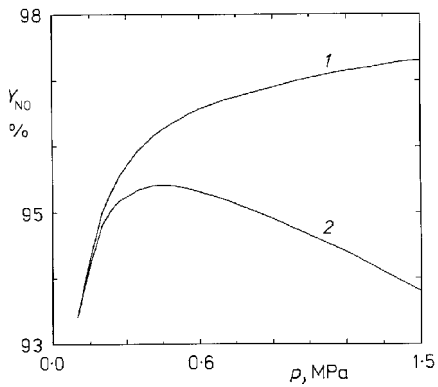

FIG. 13
Dependence of NO yield ($z = L$) on pressure for entering mixture containing 12 mole % NH_3, using models ignoring (*1*) and involving (*2*) the bulk reaction

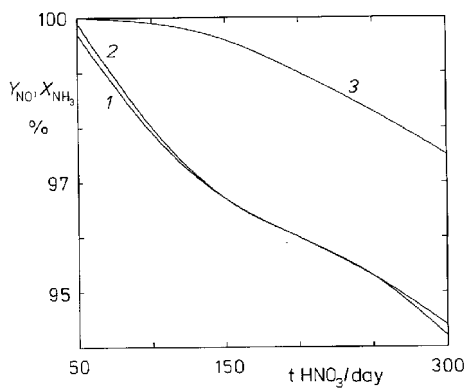

FIG. 14
Dependence of NO yield (*1*, *2*) and total NH_3 conversion (*3*) ($z = L$) on reactor load using models involving (*1*) and ignoring (*2*) the NH_3 + NO bulk reaction (total conversion (*3*) is identical for the two models)

Effect of Pressure

Calculations ignoring the reaction of NH_3 and NO in the gas phase ($R_{g,j} = 0$ in Eq. (*7*)) provided NO yields which increased with increasing pressure (Fig. 13, curve *1*), and this disagrees with reality[26]. Therefore, the mathematical model was extended with a term accounting for the reaction between NH_3 and NO in the bulk phase. The rate of that reaction, expressed by means of the kinetic equation (*3*), was inserted in the balance equation (*5*) (i = NH_3, NO). The results obtained by means of this extended model, which takes the reaction in the bulk phase into account, give NO yields which decrease if the pressure is increased above 0.4 MPa (Fig. 13, curve *2*). Hence, the decrease in the NO yield with increasing pressure, which is observed in practice, can be explained in terms of the bulk reaction of NH_3 and NO, as suggested by Carberry[17].

Effect of Reactor Load

The yield decreases with increasing reactor load (daily output in t of HNO_3), as curves *1* and *2* in Fig. 14 demonstrate. The total NH_3 conversion decreases as well (Fig. 14, curve *3*), so that in practice, unreacted NH_3 penetrates through the Pt–Rh gauzes whereby the NO yield lowers. This trend appears in both models.

CONCLUSIONS

The suggested mathematical model of a reactor with metal gauzes for the oxidation of NH_3 allows the behaviour of an experimental or industrial facility to be predicted, particularly with respect to the effect of composition and temperature of the starting reaction mixture, flow rate, and total pressure on the yield of nitric oxide and the total conversion of ammonia. An estimate of the temperature distribution in the reactor is also obtained, showing that the assumption of isothermal reaction course, which is generally adopted, is actually incorrect. Comparison of the calculated NO yields with published empirical data indicates a good agreement. The basic trends of dependences of the NO yields on the starting concentration of NH_3 and total pressure are in a reasonable agreement with published data as well. The adverse effect of total pressure on the yield can be explained in terms of increased rate of the consecutive homogeneous reaction between NH_3 and NO.

SYMBOLS

A	area of the free cross section of the catalyst bed ($\Pi\, r_1^2\, \gamma$), m^2
A_1	area of the inlet tube cross section, m^2
a_V	specific outer surface of catalyst ($a_V = S_K(1 - \gamma)/V_K$), m^{-1}
$C_{s,i}$	dimensionless concentration of component i at the catalyst surface ($C_{s,i} = c_{s,i}/c_i^0$)

c_i	concentration of component i in the gas phase, mol m^{-3}
c_i^0	concentration of component i at the reactor inlet, mol m^{-3}
$c_{s,i}$	concentration of component i at the catalyst surface, mol m^{-3}
c_p	gas thermal capacity, J mol^{-1} K^{-1}
c_{pf}	gas thermal capacity, J kg^{-1} K^{-1}
D_i	diffusion coefficient of component i, m^2 s^{-1}
d_p	characteristic dimension for the calculation of Pe_a (mean wire diameter $r_s + r_w$), m
E_i	dispersion coefficient of component i, m^2 s^{-1}
$F^0_{NH_3}$	molar flux of NH_3 at the reactor inlet ($z = 0$), mol s^{-1}
$F_{NH_3,z}$	molar flux of NH_3 at site z, mol s^{-1}
$F_{NO,z}$	molar flux of NO at site z, mol s^{-1}
G	mass flow rate of ammonia-air mixture, kg s^{-1}
h_r	radiative heat transfer coefficient ($h_r = \{0.1952/[(2/\gamma) - 0.264]\}(T^{-3}/100)$), J m^{-2} K^{-1} s^{-1}
k_{fo}	coefficient of heat transfer through the reactor wall, W m^{-2} K^{-1}
L	catalyst layer height, m
l_w	length of tightening wire per gauze mesh, m
l_s	length of closing wire per gauze mesh, m
M_i	molar mass of component i, kg mol^{-1}
N_{Nu}	modified Nuselt number for radiation ($N_{Nu} = h_r d_p/\lambda_c$)
n^0	molar flow rate at reactor inlet, mol s^{-1}
n_L	number of gauzes in catalyst bed
n_s	number of closing wires per m of gauze, m^{-1}
n_w	number of tightening wires per m of gauze, m^{-1}
Pe_a	Peclet number ($Pe_a = vd_P/E_i$)
p	pressure in reactor, Pa
p_i	partial pressure of component i, Pa
$\boldsymbol{R}$	gas constant, K mol^{-1} K^{-1}
$R_{s,j}$	rate of j-th reaction at catalyst surface, mol m^{-2} s^{-1}
$R_{g,j}$	rate of j-th bulk reaction, mol m^{-3} s^{-1}
r_1	reactor radius, m
r_s	gauze closing wire radius, m
r_w	gauze tightening wire radius, m
S_g	catalyst specific surface area, m^2 kg^{-1}
S_K	outer geometrical surface area of catalyst per m^2 gauze area, m^2 m^{-2}
T	gas temperature, K
$T = T/T_{ref}$	dimensionless temperature
T^0	gas temperature at reactor inlet, K
T_s	catalyst surface temperature, K
T_{ref}	reference temperature (T_{ref} = 750 K), K
T_v^0	gas temperature at reactor outlet, K
T_o	temperature of reactor surroundings, K
V_K	catalyst volume per m^2 gauze area, m^3 m^{-2}
v	interstitial velocity, m s^{-1}
w_i	mass fraction of component i
X_{NH_3}	total NH_3 conversion ($X_{NH_3} = (F^0_{NH_3} - F_{NH_3,z})/F^0_{NH_3}$)
X^0	NH_3 content in the entering mixture, mole%
$Z = z/L$	dimensionless axial coordinate
Y_{NO}	NO yield ($Y_{NO} = F_{NO,z}/(F^0_{NH_3} - F_{NH_3,z})$)

z	spatial axial coordinate, m
α_{fc}	fluid-catalyst heat transfer coefficient, W m^{-2} K^{-1}
α_{fo}	wall-environment heat transfer coefficient, W m^{-2} K^{-1}
α_{fw}	fluid-wall heat transfer coefficient, W m^{-2} K^{-1}
β_i	*i*-th component mass transfer coefficient, m s^{-1}
γ	gauze hole rate
$-\Delta Hr_j$	reaction enthalpy of *j*-th reaction, J mol^{-1}
λ_c	thermal conductivity of catalyst, W m^{-1} K^{-1}
λ_{ef}	effective thermal conductivity in catalyst layer, W m^{-1} K^{-1}
λ_f	thermal conductivity of gas, W m^{-1} K^{-1}
λ_s	thermal conductivity of solid, W m^{-1} K^{-1}
ρ	gas mixture density, kg m^{-3}
ρ_c	catalyst density, kg m^{-3}
$\nu_{j,i}$	stoichiometric coefficient of component *i* in *j*-th reaction
ϕ	radiation constant
ε	integral gas absorbability
σ	blackbody emission constant, W m^{-2} K^{-4}

REFERENCES

1. Atroshchenko V. I., Kargin S. I.: *Tekhnologiya azotnoi kisloty*. Nauka, Moscow 1962.
2. Satterfield C. N.: *Heterogenous Catalysis in Practice*. McGraw-Hill, New York 1980.
3. Ploskura W.: Chem. Prum. *24*, 63 (1974).
4. Regner A.: *Anorganicka technologie*. SPN, Praha 1953.
5. Vosolsobe J.: *Vyroba amoniaku a kyseliny dusicne*. SNTL, Praha 1984.
6. Dixon J. K., Longfield J. E. in: *Catalysis 7* (P. H. Emmett, Ed.). Reinhold, New York 1960.
7. Bodenstein M.: Z. Angew. Chem. *40*, 174 (1926).
8. Raschig F.: Z. Angew. Chem. *40*, 1183 (1925).
9. Zawadski J.: Discuss. Faraday Soc. *29*, 140 (1950).
10. Pignet T., Schmidt L. D.: Chem. Eng. Sci. *29*, 1123 (1974).
11. Pignet T., Schmidt L. D.: J. Catal. *40*, 212 (1975).
12. Fogel Z. M., Nadykto B. T., Rybalko Y. F., Schvachko V. I., Korobchanskaya I. E.: Kinet. Katal. *5*, 431 (1964).
13. Wise H., Frech M. F.: J. Phys. Chem. *22*, 1463 (1966).
14. Vortmeyer D.: Ger. Chem. Eng. *3*, 124 (1980).
15. Wakao N., Kato K.: J. Chem. Eng. Jpn. *2*, 24 (1969).
16. Dixon A. G., Cresswell D. L.: AIChE J. *25*, 663 (1979).
17. Carberry J. J.: *Chemical and Catalytic Reaction Engineering*. McGraw-Hill, New York 1976.
18. Satterfield Ch. N., Cortez D. H.: IEC Fund. *9*, 613 (1970).
19. Mika V., Neuzil L., Vlcek J.: *Sbirka prikladu z chemickeho inzenyrstvi*. SNTL, Praha 1981.
20. Armour J. C., Cannon J. N.: AIChE J. *14*, 415 (1968).
21. Villadsen J., Michelsen M.: *Solution of Differential Equation Models by Polynomial Approximation*. Prentice Hall, New York 1978.
22. Ried C. R., Prausnitz J. M., Sherwood K. T.: *The Properties of Gases and Liquids*. McGraw-Hill, New York 1977.
23. Anderson D. R.: J. Catal. *113*, 475 (1988).
24. Zabryeski J., Zmyslony R.: Appl. Catal. *35*, 13 (1987).

25. Busby J. A., Knapton A. G., Budd A. E. R.: *Proc. Fertiliser Soc. 169*. London 1978.
26. Karavaev M. M., Zasorin A. P., Kleshchev M. F.: *Kataliticheskoe okislenie ammiaka*. Khimiya, Moscow 1983.

Translated by P. Adamek.